scientific reports

Check for updates

OPEN

Two paired HPV-59 cervical cancer cell lines with distinct chemoradioresistant phenotypes

Irina Tatarnikova[1], Vadim Talyshev[1], Aleksandra Sen'kova[1], Oleg Markov[1], Darya Mikhailova[1,2], Oksana Pashkovskaya[3], Sergey Krasilnikov[2], Elena Samoilova[3], Tatyana Gainer[1,4], Evgeniy Brener[1], Marina Zenkova[1] & Evgeniya Logashenko[1]✉

Cervical cancer (CC) is the fourth most common cancer among women worldwide and a leading cause of cancer-related death. While immortalized cell lines like HeLa are widely used, they often lose characteristic features of the original tumor due to long-term cultivation. Primary cell cultures offer a more representative model, as they retain key features of the native tumor microenvironment. Here, we establish and characterize two novel human CC cell lines, AdMer35 and AdMer43, uniquely derived from paired tumor biopsies of the same patient before (AdMer35) and after (AdMer43) chemoradiotherapy for stage IIIB squamous cell carcinoma. Both lines exhibited stable epithelial morphology (cobblestone pattern), adhesion, were positive by cytokeratin staining, and have HPV-59 DNA genomes. They displayed distinct karyotypes: 80% of AdMer35 cells were near-tetraploid (modal number 95), while 98% of AdMer43 cells were near-triploid (modal number 77). Functional assays revealed significant differences: AdMer43 proliferated faster (Cell Index ~ 3.8 vs. ~2.1 at 100 h), but AdMer35 migrated more rapidly. Crucially, AdMer43 demonstrated increased resistance in comparison with AdMer35 to both radiotherapy (minimal apoptosis and G2/M arrest post-5 Gy irradiation) and chemotherapy (IC_{50} for carboplatin: 87.8 µM vs. 54.3 µM; for paclitaxel: 7.3 nM vs. 3.0 nM). Both lines were tumorigenic in nude mice, forming histologically distinct tumors. Thus, we present a novel paired in vitro model of acquired chemoradioresistance in cervical cancer. The AdMer35/AdMer43 cell line pair provides a unique tool for mechanistic studies of therapy resistance and preclinical drug screening.

Keywords Cervical cancer, Chemoradioresistance, Primary culture, Gynecological cancer, HPV

Cervical cancer (CC) is the fourth most common oncological disease among women worldwide and remains one of the leading causes of cancer-related deaths in women[1]. Over the past 30 years, the incidence rate of CC in women in the 15–49 age group has been steadily increasing worldwide[2,3]. The primary cause of CC is persistent infection with high-risk HPV types, with HPV16 and HPV18 accounting for ~ 70% of cases. While the causal link between oncogenic HPV and CC is well established, the early events of HPV-driven carcinogenesis and the precise cellular origins of CC remain poorly understood[4–6]. Additionally, other risk factors, including reproductive and sexual behavior and lifestyle-related factors, may also contribute[7].

Current treatment protocols for CC include radiotherapy, surgery, chemotherapy, targeted therapy, and immunotherapy[8,9]. Due to the radiosensitivity of tumor cells, combined chemoradiation is a widely used and effective strategy[10]. However, despite advances in CC therapy, outcomes remain suboptimal. Recent data show that, unlike most cancers, the survival rate for patients with uterine malignancies, including CC, has not improved significantly in the past four decades. Even in specialized oncology centers, the 5-year survival rate remains around 67%, primarily due to treatment failure and the development of chemoradioresistance[11].

Immortalized CC cell lines such as HeLa are important tools in basic and translational research. However, the number of available CC lines is limited, and many are affected by cross-contamination, misidentification, or extensive in vitro adaptation, limiting their utility in modeling the biological complexity of CC[12–14]. In contrast, primary CC cell cultures preserve key characteristics of the original tumor, including epithelial morphology,

[1]Institute of Chemical Biology and Fundamental Medicine Siberian Branch Russian Academy of Sciences, Novosibirsk, Russian Federation. [2]Novosibirsk National Research State University, Novosibirsk, Russian Federation. [3]Meshalkin National Medical Research Center, Ministry of Health of the Russia, Novosibirsk, Russian Federation. [4]Research Institute of Clinical and Experimental Lymphology, Novosibirsk, Russian Federation. ✉email: evg_log@1bio.ru

tumor heterogeneity, and stem-like features. For instance, primary cultures can display a side population with high clonogenicity and tumorigenicity[15], and may even simultaneously exhibit cancer stem-like and fibroblast-like features[16,17]. Distinct molecular and phenotypic properties have been reported between different histological variants of CC. For example, exophytic tumors express higher levels of VEGF-A and EGF, while endophytic tumors show increased VEGF-D expression[18]. Other studies show that cervical precancerous cells proliferate faster than normal cells but slower than CC cells[19], and that chromosomal instability increases with tumor stage and differs between squamous and glandular tumors[20]. They also noted differences between squamous cell carcinomas and adenocarcinomas. Deng et al. developed an optimized method for culturing epithelial cells from different cervical regions, including the transformation zone, which is highly susceptible to carcinogenesis[21].

The lack of cervical cancer cell models obtained from the same patient at different treatment stages represents a gap that hampers the study of resistance development.

In this study, we established and characterized two CC cell cultures, AdMer35 and AdMer43, derived from tumor biopsies obtained from the same patient before and after radiotherapy. After long-term propagation, both cultures demonstrated stable growth, epithelial phenotype, and tumorigenicity in nude mice. Based on accepted criteria (including morphological stability, cytokeratin expression, HPV status, and ability to survive freeze–thaw cycles), these models can be classified as established cell lines. Despite their common origin, AdMer35 and AdMer43 exhibit marked differences in proliferation, migration, response to chemo- and radiotherapy, and Ki67 expression, providing a rare and valuable in vitro model to study treatment-induced phenotypic shifts and acquired resistance in cervical cancer.

Results

Clinical characterization and establishment of a primary cell culture

From January 2022 to June 2024, 45 cervical tumor biopsies were processed (Table S1). Only two (4.4%) cell cultures, named AdMer35 and AdMer43, had epithelial phenotypes, proliferated for more than 12 months, survived, and continued to grow after several freezing-thawing cycles. Both cell lines were derived from a 22-year-old patient after whom the line is named. The patient was diagnosed with stage IIbN1M0 (IIIB) squamous cell carcinoma of the cervix, exophytic form, vaginal-parametrial variant. The disease was diagnosed in June 2023. A tumor tissue sample was collected from the patient during a routine visit to the Academician E.N. Meshalkin National Medical Research Center. The primary culture AdMer35 was subsequently developed from this sample.

In November and December 2023, the patient received concurrent chemoradiation. Subsequently, another tumor tissue sample was collected in March 2024, resulting in the development of the primary culture AdMer43 (for details, see Supplementary, Therapy schedule for AdMer patient).

Cell cultures AdMer35 and AdMer43 grew attached to the flask, and cells formed an irregular island pattern with a cobblestone morphology, which is characteristic of epithelial cells (Fig. 1A and B). AdMer35 and AdMer43 were larger in comparison with well-studied SiHa and HeLa CC cells (Fig. 1C and D). Also, in the field of view, there were single spindle-shaped cells visually resembling fibroblasts. It was found that unlike SiHa and HeLa cells (Figure S1, C–D), AdMer35 and AdMer43 cells were not forming well-defined cell colonies (Figure S1, A–D). When AdMer35 and AdMer43 cells reached confluence, cells were frozen in DMEM supplemented with 30% FBS and 10% DMSO in liquid nitrogen and stored for further assays.

HPV status and genotyping

We evaluated the presence of the HPV genome in the AdMer35 and AdMer43 cells. For this purpose, the RealBest DNA HPV HR screen assay was used. The positive fluorescence signal in the ROX channel witnessed the presence of HPV of either of the HPV 31, 35, 39, 45, 51, 52, 56, 58, 59, 66, 68 genotypes. To identify which high-risk HPV type was present in the cells, a genotyping test was performed using the RealBest DNA HPV HR genotype assay. Performed analysis shows that in AdMer35 and AdMer43 cells, HPV type 59 is present.

Immunophenotypic characterization

A tumor tissue sample contains not only cancer cells but also stromal cells, which mainly consist of fibroblasts. In order to differentiate epithelial cells from fibroblasts, AdMer35 and AdMer43 cells, as well as hFF3 fibroblast cells, were stained with monoclonal antibodies to cytokeratin and fibronectin. AdMer35 and AdMer43 cells were characterized by strong cytokeratin expression, while no fibronectin expression was detected (Fig. 1E and G). On the other hand, the hFF3 fibroblasts used as a control exhibited the opposite staining pattern, with strong fibronectin expression but no cytokeratin expression. Although both AdMer35 and AdMer43 cells were cytokeratin positive, the degree of fluorescence differs (Fig. 1E and F). Using flow cytometry, we showed that indeed, 100% of cells of both types contain a cytokeratin signal, but in the case of AdMer35 cells, we see one peak with a mean fluorescence value equal to 4.1×10^4 RFU, while in the case of AdMer43, 12% of cells are characterized by the mean fluorescence value of 2.6×10^4 RFU, and 88% of cells – by a value equal to 28×10^4 RFU (Fig. 1F). Thus, a more pronounced expression of cytokeratin is observed in AdMer43 cells compared to AdMer35. Also, we showed that AdMer35 and AdMer43 cells did not express fibronectin because fibronectin-specific fluorescence within cells did not differ from the control (non-stained cells), while fibroblasts hFF3 were characterized by high fibronectin expression amounting to 57.8×104 RFU (Fig. 1H). The data indicate that both the established cell lines, AdMer35 and AdMer43, are epithelial ones.

Chromosome analysis

The complicated karyotype and abnormal chromosome number of the AdMer35 and AdMer43 cells were revealed by chromosome analysis (Fig. 2A and B). Most of the examined AdMer35 cells (80%) were near-tetraploid (Fig. 2A, Table S2), with chromosomal numbers ranging from 81 to 100. In addition, 6% and 14% of the cells were near-diploid and near-triploid, with chromosomal numbers ranging from 51 to 56 and 58 to

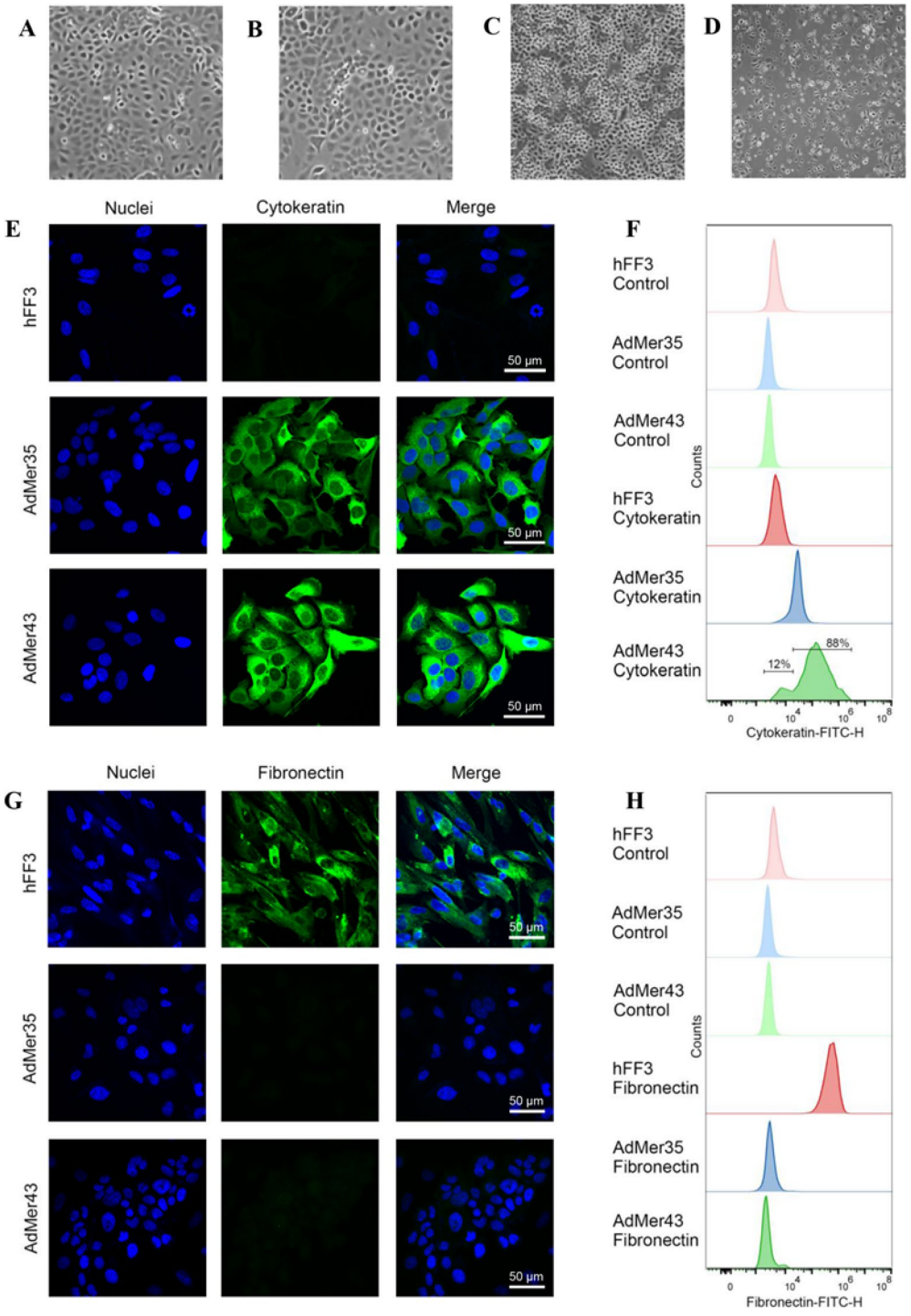

Fig. 1. AdMer35 and AdMer43 cells characterization. (**A**–**D**) Morphology of cervical cancer cells AdMer35, AdMer43, SiHa and HeLa (respectively). All pictures were taken under inverted phase contrast microscope (EVOS XL Core×4). Expression of cytokeratin and fibronectin in human fibroblasts hFF3 and human CC cells AdMer35 and AdMer43 was measured after cell staining with primary anti-Cytokeratin (**E**, **F**) or anti-Fibronectin (**G**–**H**) monoclonal antibody followed by staining with secondary polyclonal anti-hIgG- AF488 antibody (green channel). Microphotographs (**E**, **G**) were captured with a Zeiss LSM710 confocal microscope using a Plan-Apochromat 63×/1.40 Oil DIC M27 objective. Nuclei were stained with DAPI (blue channel). FACS analysis (**F**, **H**) was performed with NovoCyte 3000 flow cytometer, 10.000 events were acquired for each sample. The data were processed using NovoExpress software.

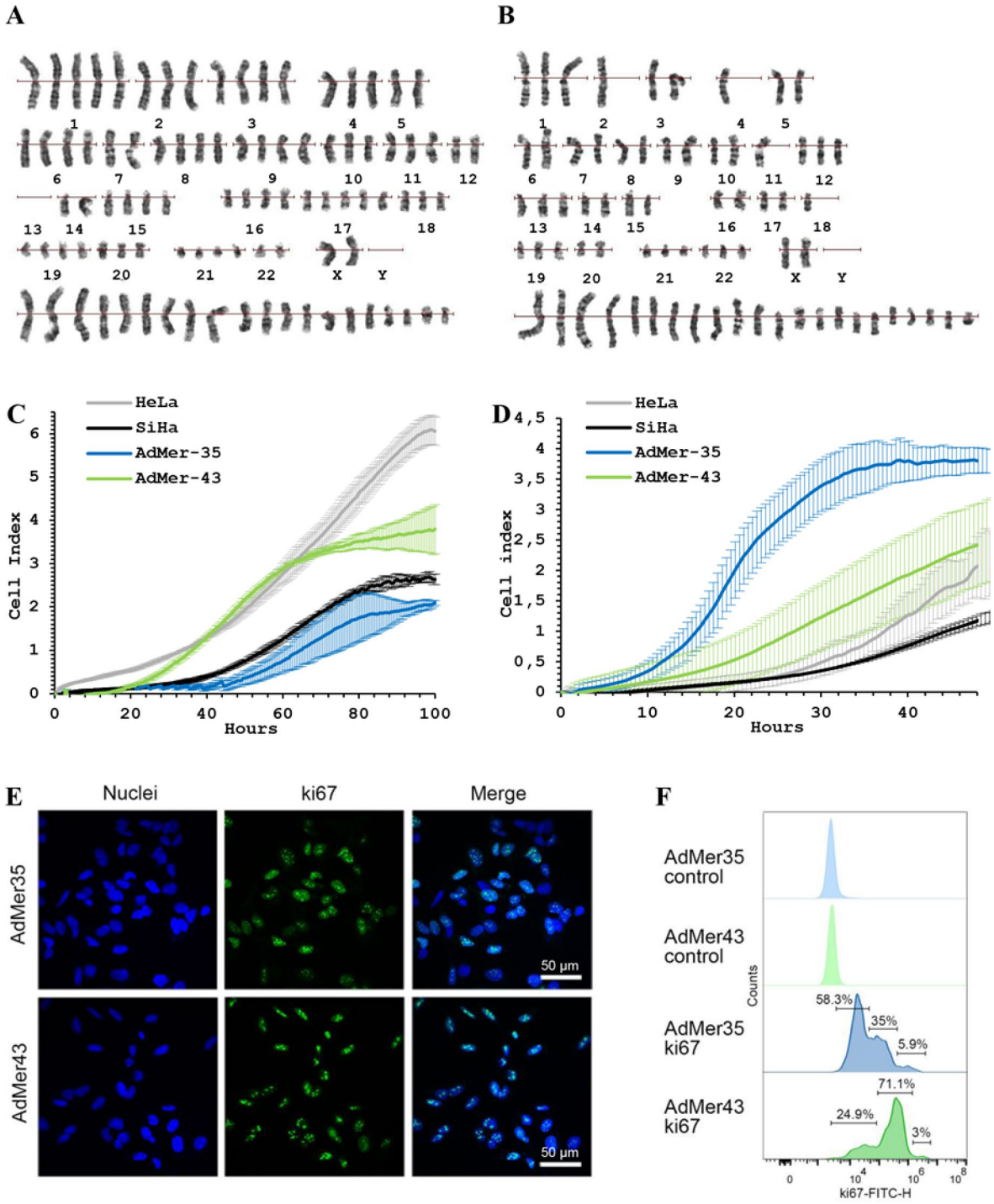

Fig. 2. AdMer35 and AdMer43 cells characterization. (**A**) AdMer35 and (**B**) AdMer43 cells karyotypes, GTG staining. Proliferation (**C**) and migration (**D**) activity of HeLa, SiHa, AdMer35 and AdMer43 cells monitoring using xCELLigence RTCA system. Data were recorded once per 30 min during 100 h and expressed as Cell index. (**E**, **F**) Expression of ki67 in human cervical cancer cells AdMer35 and AdMer43 was measured after cell staining with primary anti-Ki67 monoclonal antibody followed by staining with secondary polyclonal anti-hIgG- AF488 antibody (green channel). Microphotographs (**E**) were captured with a Zeiss LSM710 confocal microscope using a Plan-Apochromat 63×/1.40 Oil DIC M27 objective. Nuclei were stained with DAPI (blue channel). FASC analysis (**F**) was performed with NovoCyte 3000 flow cytometer, 10.000 events were acquired for each sample. The data were processed using NovoExpress software.

79, respectively. The modal number of chromosomes was 95. Unlike AdMer35, the vast majority of examined AdMer43 cells (98%) were near-triploid (Fig. 2B, Table S2) with chromosomal numbers ranging from 69 to 80, and only 2% of cells were near-tetraploid (chromosomal numbers 84). The modal number of chromosomes was 77.

Five metaphase plates for each line were analyzed using GTG differential staining. All plates showed multiple chromosomal rearrangements. The rearranged chromosomes in the karyograms were located on the lower line (Fig. 2A-B).

Proliferation and migration potential, tumorsphere formation

The growth and migration potential of AdMer35 and AdMer43 cells were assayed by xCELLigence Real-Time Cell Analysis using HeLa and SiHa cells as controls (Fig. 2C–D). A wound healing assay was also conducted to assess migration potential (Figure S3). The AdMer35 and AdMer43 cells showed different growth rate profiles. AdMer43 cells similar to HeLa grew rapidly for more than 60 h and reached a cell index (CI) of 3.2, after which the proliferation rate slowed significantly. The AdMer35 cells were in the exponential growth phase for 80 h and reached a CI of 1.7. At the 100 h time point, the CI of AdMer43 also was twice as high as that of AdMer35 cells (3.8 vs. 2.1, respectively). The opposite situation was observed when comparing the migration rates of these lines (Fig. 2D, Fig. S3). AdMer35 cells migrated rapidly, and almost all AdMer35 cells migrated within 32 h, and the plateau of the curve was reached at CI 3.5. Opposite to AdMer35, AdMer43 cells exhibited a slow migration rate, a smooth migration curve was observed during the entire 48 h of observation, reaching CI 2.4. It is noteworthy that the slope of the growth curve for AdMer43 and HeLa coincides in the segment up to 60 h, after which AdMer43 reaches a plateau, and HeLa continues to grow exponentially. This may be due to different cells sizes: AdMer43 are much bigger than HeLa (Fig. 1B and D) and by 60 h, AdMer43 apparently fills the entire area of the well, while HeLa cells were still growing. So, as soon as the confluence is reached, the CI did not change, showing a plateau since upon xCELLigence Real-Time Cell Analysis the occupancy of the well is measured.

Comparison with the well-known CC cell lines HeLa and SiHa shows that the new cell lines occupy intermediate positions in terms of proliferation rate: AdMer35 < SiHa < AdMer43 ≈ HeLa, but exhibit much higher migratory activity: SiHa < HeLa < AdMer43 < AdMer35 (Fig. 2C and D).

Ki67 is an ideal molecular marker showing tumor cell proliferative potential. Ki67 expression is associated with tumor proliferation, invasion, metastatic potential, and prognosis[22]. Both cell lines are characterized by strong and diffuse nuclear staining with Ki67 monoclonal antibodies, moreover, Ki67 staining is not evenly distributed among the cell population (Fig. 2E). The detailed analysis of Ki67 expression by flow cytometry revealed that both cell lines, AdMer35 and AdMer43, are not homogeneous in marker expression, and in each case, there are at least three cell populations that differ in the level of Ki67 expression (Fig. 2F). The average Ki67-positive mean fluorescence intensity (MFI) for AdMer35 is 11.1×10^4 RFU; the majority of these cells, 58.5%, are characterized by the MFI of 1.9×10^4 RFU, for 35% this parameter is 12.2×10^4 RFU, and for 5.9% it is 91.7×10^4 RFU. For AdMer43 cells, the average MFI value is more than 3 times higher than for AdMer35 and is 36.1×10^4 RFU. In this case, most cells, 71.6% express the Ki67 protein at a level of 39.3×10^4RFU, 25.4%- 3.3×10^4 RFU and 3%- 200×10^4 RFU. Results on Ki67 expression correlate with the proliferation assay showing much higher proliferative potential of AdMer43 cells compared with AdMer35 cells.

Moreover, we showed that both AdMer35 and AdMer43 cells were shown to form tumorspheres (Figure S4), providing indirect confirmation that both cell lines contain cancer stem cells. However, the morphology of the tumorspheres differed between the cell cultures. Specifically, AdMer35 formed large (150–200 μm in diameter) tumorspheres with irregular borders. In contrast, AdMer43-derived tumorspheres were smaller (approximately 100 μm in diameter) with a smooth, well-defined periphery (Figure S4) and were often surrounded by small clusters of aggregated cells (Figure S4).

Chemoradiosensitivity of AdMer35 and AdMer43 cell lines

As mentioned above, cells AdMer35 and AdMer43 were obtained at different stages of the tumor progression. For AdMer35, the tumor sample was withdrawn before radiotherapy, and the tumor sample for AdMer43 – after the end of two courses of radiotherapy. Therefore, it was interesting to compare the response of these established cells to irradiation.

Since the SFD used for the patient's intracavitary brachytherapy was 5 Gy (see Supplementary, Therapy schedule for AdMer patient), this is the radiation dose we used in experiments.

The proliferation of new cell lines before and after irradiation was analyzed by xCELLigence Real-Time Cell Analysis (Fig. 3A, Figure S2, C and D). After a single irradiation (5 Gy) the growth rate of irradiated and intact AdMer35 cells did not differ during 48 h, after which intact cells proliferated rapidly, reaching a plateau at CI 1.7 after 80 h, while the irradiated cells grew slowly throughout the entire observation time (100 h) (Figure S2, C). At the end point of measurement, the differences in the CI for intact and irradiated AdMer35 cells differed more than 2-fold (1.7 vs. 0.7, respectively) (Fig. 3A). As for AdMer43 cells, the growth rate of irradiated and intact (control) cells did not differ up to 60 h, and at the 100 h time point, the CI of control and irradiated cells differed by not more than by 1.2 fold (3.5 vs. 2.9, respectively) (Fig. 3A). In the case of HeLa and SiHa cells, a trend similar to AdMer35 was observed, specifically, up to 48 h the growth rate of control and irradiated cells was similar, but at the end point of measurement (100 h) it differed by approximately 2-fold (CI 2.4 vs. 1.1 for SiHa and 4.6 vs. 2.3 for HeLa).

Cell viability was assessed 4 and 6 days after X-irradiation using the LDH test. We selected the lactate dehydrogenase (LDH) assay to evaluate the cytotoxic effects of ionizing radiation, as it directly measures cell plasma membrane disintegration in dying cells, which results in the release of cytoplasmic enzymes such as LDH that can be easily measured to quantify the number of dead cells in vitro[23]. Unlike metabolic assays such as MTT, the LDH assay provides a more accurate and reproducible assessment of cell viability under radiation-induced

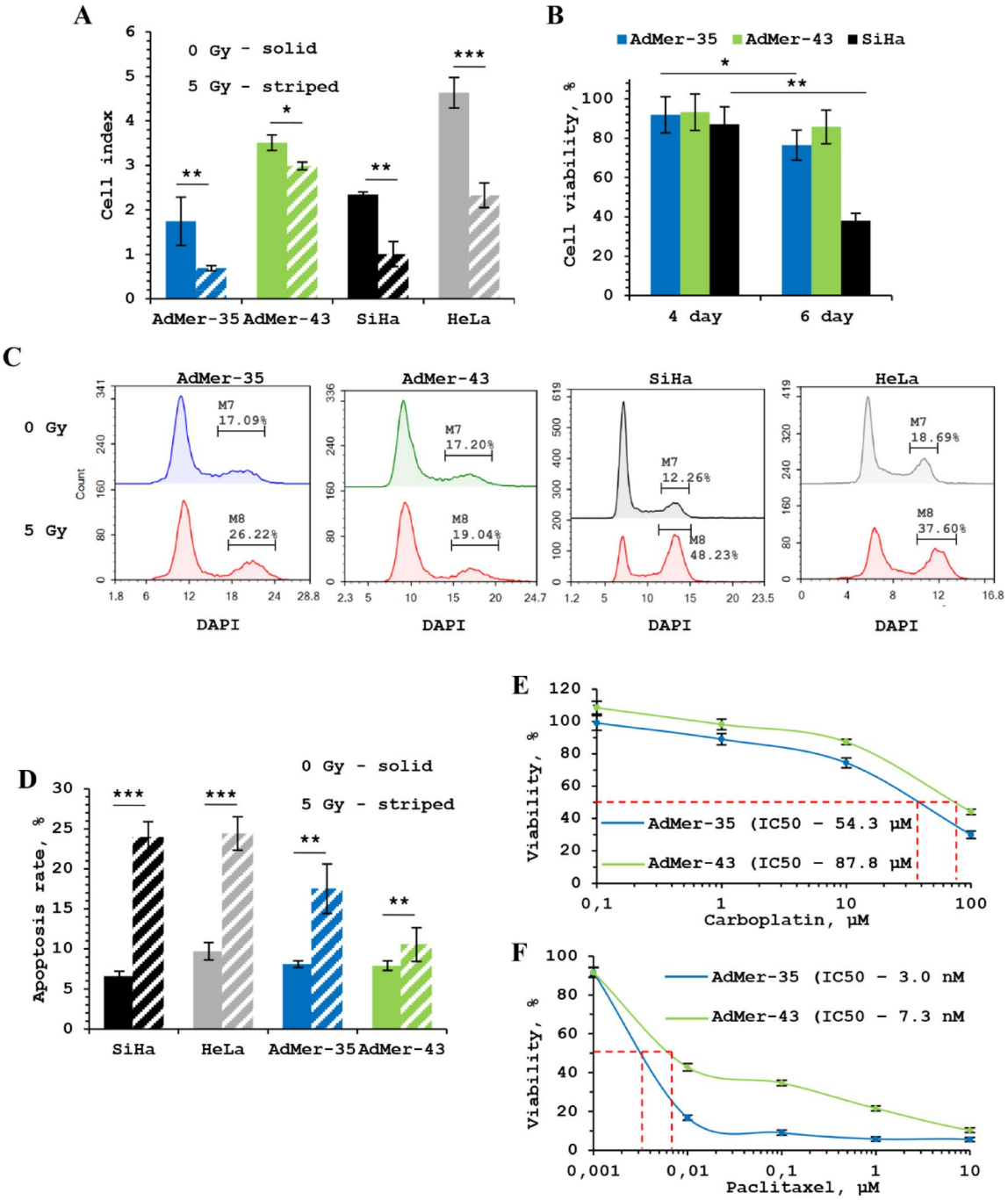

Fig. 3. Radiation and chemotherapy effects on CC cell lines HeLa, SiHa, AdMer35 and AdMer43. (**A**) Proliferation of intact and irradiated (5 Gy) cancer cells monitoring using xCELLigence RTCA system. Data were recorded once per 30 min during 80 h and expressed as Cell index at 80 h point. (**B**) Viability of cells, measured by lactate dehydrogenase (LDH) activity in the cells conditioned medium 4 and 6 days after irradiation using the CyQUAN LDH Cytotoxicity Assay kit as described in the Materials and methods section. Non-irradiated cells were used as a control. Data were obtained from three separate experiments in triplicate. (**C**) Cell cycle phase distribution of cells 24 h after 5 Gy irradiation measured by DAPI staining. Fluorescence was captured with NovoCyte 3000 flow cytometer. The signal was detected in pacific blue channel. Histograms of cell cycle stages distribution were acquired with NovoExpress Software. (**D**) Radiation-induced apoptosis measured by Annexin V-FITC/PI apoptosis detection kit staining 5 days after irradiation, flow cytometry data. (**E**) Carboplatin and (**F**) Paclitaxel effects on AdMer35 and AdMer43 cell viability. Cells were incubated for 72 h with increasing concentrations of carboplatin (0.1 to 100 μm) or paclitaxel (0.001 to 10 μm). Cell viability was measured by the MTT assay as described in the Materials and methods section. The results are expressed as percentages of viable cells observed after treatment, relative to control cells (100%) incubated in the complete DMEM. Data were obtained from three separate experiments in triplicate. (*-$p < 0.05$, **-$p < 0.01$, ***-$p < 0.001$)

stress[24]. Four days after irradiation, no significant decrease in cell viability was observed for both new and control (SiHa) cells. After 6 days, the proportion of living cells was 75% and 86% for AdMer35 and AdMer43, respectively, while only 38% of SiHa cells were alive (Fig. 3B).

Flow cytometry was used to analyze radiation-induced cell cycle changes at 0 and 24 h after irradiation using DAPI staining. The results are depicted in Fig. 3C. Without irradiation, all cells showed approximately equal distribution across cell cycle phases, with a significant predominance of cells in G1-phase. Following irradiation, a decrease of cells in G1-phase and a significant increase in the number of HeLa and SiHa cells in the G2/M-phase were observed (48% and 38% vs. 12% and 19% without irradiation, respectively), indicating DNA damage[25,26]. In contrast, in the case of AdMer35 and AdMer43 cells, the number of cells in the G2/M phase increased 1.5-fold for AdMer35 (26% vs. 18%), while for AdMer43 it remained unchanged compared to the control. No subG1 population was observed 24 h after irradiation in all cell lines tested.

Irradiation may induce various cell killing effects, such as apoptosis, necrosis (including necroptosis), autophagy, senescence, and mitotic catastrophe[27]. Apoptosis and necrosis are the most important types of irradiation-induced cell death. Therefore, the classic method of apoptosis and necrosis detection – annexin V and PI double staining was applied to detect the changes in the number of apoptotic and necrotic cells after radiation. Radiation-induced apoptosis was not observed 1 day after irradiation in any of the cell lines (Figure S5). The annexin-V staining population ((annexin V + PI−) and (annexin V + PI+)) increased to 25% in response to 5 Gy in SiHa and HeLa cells 5 days after irradiation (Fig. 3D). For AdMer35 cells the increase of the annexin-V population was 17%, whereas in the case of AdMer43 cells, only 2% of the cells were Annexin-V + compared to the control. It should be noted that no increase in necrotic cell counts (annexin V − PI+) was detected for any cell line after irradiation.

Both the AdMer35 and AdMer43 cell lines were obtained after polychemotherapy was administrated according to the scheme of paclitaxel combined with carboplatin, so we investigated whether these cells developed resistance to these drugs. The ability of carboplatin and paclitaxel to suppress the growth of CC cells was tested using the MTT assay. The results of the experiment are shown in Fig. 3E and F. The response to paclitaxel and carboplatin was dose-dependent, and AdMer35 cells were more sensitive to both drugs than AdMer43: the IC_{50} values for AdMer35 and AdMer43 for carboplatin was 54.3 μM vs. 87.8 μM, respectively, and for paclitaxel 3.0 nM vs. 7.3 nM, respectively.

Assessment of tumorigenicity and histological structure of primary cell cultures AdMer35 and AdMer43

The tumorigenicity of AdMer35 and AdMer43 cells was studied by generating primary tumor nodes in athymic Nude mice by subcutaneous implantation of tumor cells at a dose of 2× and 3×10^6 cells per mouse. The development of tumors was monitored for 21 days, then tumors were excised and analyzed. As shown in Fig. 4A and D (left panels), well-defined tumor nodes were formed on day 21 after implantation of both AdMer35 and AdMer43 cells, represented by small nodule conglomerates with clear borders and a rounded or elongated shape.

Assessment of tumor growth in dynamics demonstrates only slight differences depending on the number of implanted cells at the initial stages of tumor development, but after day 10 of tumor growth, more intensive enlargement of both AdMer35 and AdMer43 inoculated at a dose of 3×10^6 cells per mouse compared to those of 2×10^6 cells per mouse was detected (Fig. 4A and D, middle panels). However, statistically significant differences in tumor growth dynamics were found only for AdMer35: the volumes of primary tumor nodes formed by AdMer35 cells were 4.2- and 2.5-fold larger in 3×10^6 cells/mouse grafting compared to 2×10^6 cells/mouse on days 14 and 21, respectively (Fig. 4A, middle panel). Evaluation of the tumor weights of AdMer35 and AdMer43 at the end of the experiment showed a 3.2- and 4.4-fold increase in this parameter when tumor cells were implanted at a higher dose (3×10^6 cells/mouse) in comparison with a lower dose (2×10^6 cells/mouse), but the differences were not statistically significant (Fig. 4A and D, right panels).

Upon a more thorough assessment of the growth dynamics of the tumors studied, attention is drawn to the faster and more intensive growth of AdMer35 compared to AdMer43: the sizes of the primary tumor nodes formed by AdMer35 cells reached 356.7 ± 43.7 mm^3, while this parameter for AdMer43 was 127.6 ± 55 mm^3, when both cell cultures were implanted at a dose of 3×10^6 cells/mouse on day 21 of tumor growth (Fig. 4A and D, middle panels). Moreover, it is worth mentioning the heterogeneity in size and weight of tumors formed (Fig. 4A and D) may be related to the individual characteristics of the immune status of the mice used in this study, since the athymic mice may contain both remnants of T-cell immunity and fully intact B-cell immunity. If the extreme points (the smallest and the largest tumors) are excluded from the analysis, then in general the sizes of the tumor nodes will be nearly the same regardless of the implanted cell dose. Nevertheless, despite the mentioned development features of tumors formed by AdMer35 and AdMer43 cells, both cell cultures demonstrate tumorigenic potential in Nude mice.

Histologically, primary tumor nodes formed by AdMer35 and AdMer43 cells were represented by polymorphic undifferentiated cells with well-defined cytoplasm with vacuoles, up to giant forms, which corresponds to the picture of a malignant tumor of epithelial origin (Fig. 4B and E, left panels). Tumor nodes have a well-formed fibrous capsule, as well as connective tissue streaks extending from it, penetrating the tumor and giving it a honeycomb structure (Fig. 4B and E, right panels). It should be noted that the stromal component was more pronounced in tumor nodes formed by AdMer43 cells than AdMer35: this tumor tissue was completely permeated with connective tissue fibers forming a thigh network with islets of single tumor cells (Fig. 4E, right panel).

The mitotic activity of both AdMer35 and AdMer43 tumors was approximately the same and generally did not depend on the number of tumor cells transplanted. The numerical density of tumor cells in the state of mitosis in AdMer35 tumor tissue was 4.1 ± 0.9 and 3.9 ± 0.5 per test area for dose 2 and 3×10^6 cells/mouse,

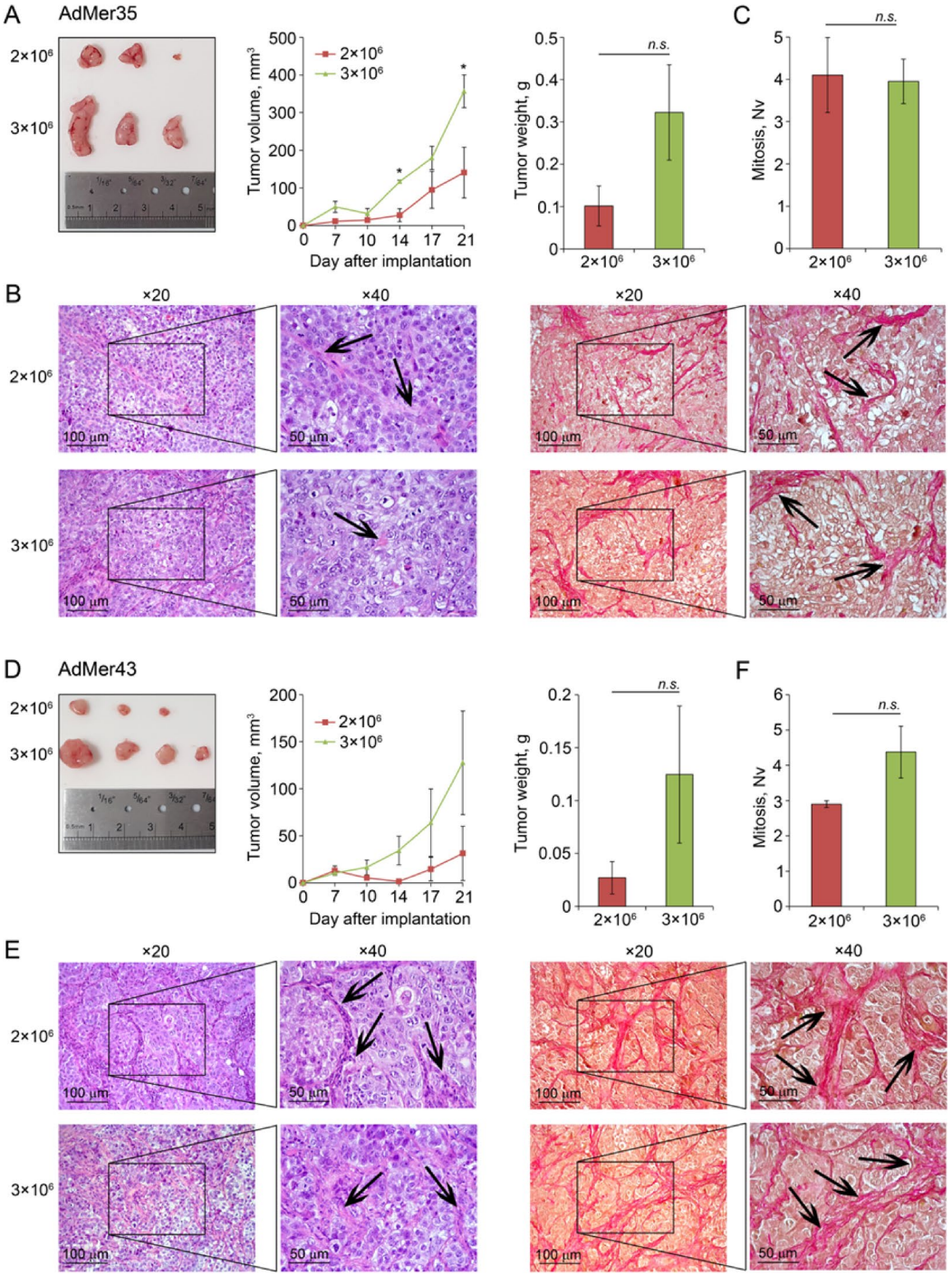

Fig. 4. Tumorigenicity of AdMer35 and AdMer43 CC cells. (**A**, **D**) Primary tumor nodes (left panel), tumor volume (middle panel), and tumor weight (right panel) of AdMer35 **(A)** and AdMer43 **(D)**, respectively. Cells were implanted subcutaneously at doses of 2× and 3×10^6/mouse in Nude mice ($n = 3$ to 4). **(C**, **F)** Mitotic activity of AdMer35 **(C)** and AdMer43 **(F)**. Numerical density (Nv) of mitosis shows the number of cells in mitosis in the square unit, 3.2×10^6 µm^2 in this case. (**B**, **E**) Representative histological images of AdMer35 (**B**) and AdMer43 (**E**) tumors, respectively. Hematoxylin and eosin staining (left panels), Van Gieson staining (right panels). Original magnification ×200 and ×400. The black boxes show areas examining at a higher magnification. The black arrows indicate connective tissue fibers in the tumor tissue. n.s. – statistically insignificant differences.

respectively (Fig. 4C). The numerical density of mitosis in AdMer43 tumor tissue was 2.9 ± 0.1 and 4.4 ± 0.7 per test area for doses 2× and 3 × 10^6 cells/mouse, respectively (Fig. 4F).

Immunohistochemical staining of AdMer35 and AdMer43 primary tumor nodes with anti-cytokeratin primary antibodies showing total cytokeratin expression by tumor cells confirmed their epithelial origin, which is fully consistent with in vitro data (Fig. 5A and C). Immunohistochemical staining of AdMer35 and AdMer43 tumors with primary antibodies to the proliferation marker Ki-67 shows their high proliferative activity in Nude mice, with AdMer43 having a much more pronounced proliferative rate compared to AdMer35, regardless of the dose of implanted cells (Fig. 5B and D). The numerical density of Ki-67 positive cells in primary AdMer35 tumor nodes was 13.7 ± 3 and 11.8 ± 2.1 cells per test area, while this parameter in primary AdMer43 tumor nodes was 3.2- and 3.7-fold higher than in AdMer35 amounting to 44.1 ± 4.6 and 43.7 ± 9.5 per test area when implanting 2× and 3 × 10^6 cells/mouse, respectively (Fig. 5B, right panel).

Discussion

The establishment of new CC cell lines is crucial for advancing our understanding of CC biology, particularly in the context of radio and drug resistance mechanisms. Currently, the field relies heavily on a limited number of widely used CC cell lines. Although these cell lines have significantly contributed to CC research, they present certain limitations that may hinder a comprehensive understanding of the disease's heterogeneity. In addition, many of these cell lines have been extensively passaged, leading to genetic drift and potentially reducing their relevance to the original tumor.

In the present study, we successfully established and characterized two new CC cell lines, AdMer35 and AdMer43, that were obtained from a patient with squamous cell carcinoma of the cervix before and after radiation therapy. As far as we know, this is the first documented paired-cell model of cervical cancer, providing a unique opportunity to separate treatment-induced molecular and genomic adaptations from genetic variation. The obtaining of new patient-derived CC cell lines and organoids is critical for the development of personalized therapies. These models preserve the specific HPV integration sites, somatic mutations, and molecular subtypes of the patient's original tumor, providing a more robust platform for drug discovery. Studies using these new models enable the investigation of chemoradioresistance mechanisms in the context of a specific patient and the screening of drugs and/or drug combinations that can sensitize therapy-resistant tumors[28,29]. Moreover, the

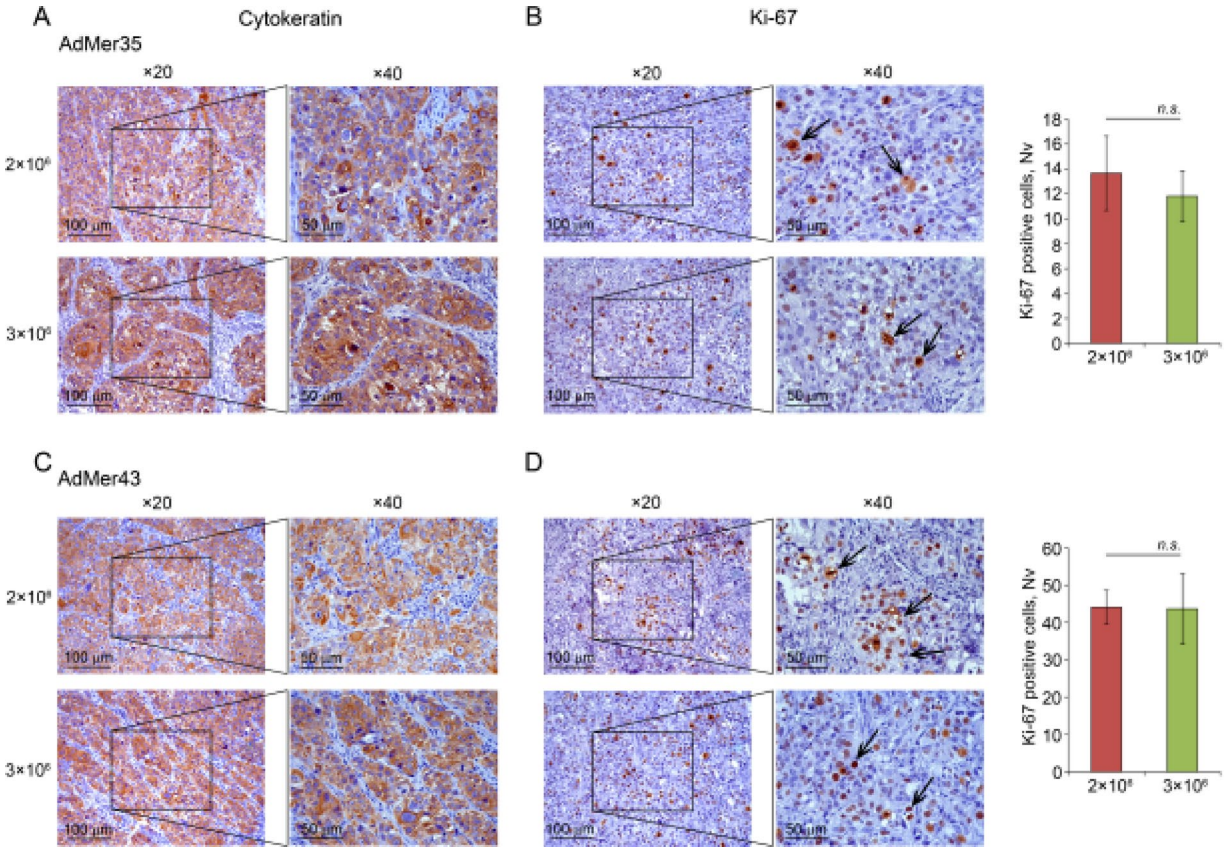

Fig. 5. Immunohistochemical staining of tumor sections ($n = 3$) of AdMer35 (**A**, **B**) and AdMer43 (**C**, **D**) primary tumor nodes with anti-cytokeratin (**A**, **C**) and anti-Ki-67 (**B**, **D**) antibodies. Original magnification ×200 and ×400. The black boxes show areas examining at a higher magnification. The black arrows indicate Ki-67 positive cells. Numerical density (Nv) of Ki-67 positive cells shows the number of studied cells in the square unit, 3.2 × 10^6 µm^2 in this case.

Characteristic	AdMer35	AdMer43
HPV status	HPV 59	HPV 59
Immunophenotypic characterization	cytokeratin^{+}fibronektin^{-}	cytokeratin^{+}fibronektin^{-}
Chromosome analysis	near-tetraploid	near-triploid
Proliferation potential in vitro	+[1]	+++[1]
Ki67 expression	Ki67^{+}	Ki67^{+}
Migration potential (time for 100% to migrate)	32h[2]	> 50h[2] (not achieved)
Tumorigenicity in mice	+	+
Radio sensitivity	yes	no
Chemosensitivity, IC50[3]		
Paclitaxel	3.0 nM	7.3nM
Carboplatin	54.3 nM	87.8 nM
Tumorsphere formation	+	+

Table 1. Summary points. [1] – the time to reach CI 1 was 36 h for AdMer43 and 68 for AdMer35. [2] – time it takes for 100% of cells to migrate. [3] – concentration required to decrease cell viability to 50%.

ability to culture cells from rare and aggressive subtypes provides a unique opportunity to study their biology and test targeted therapies in cases where clinical trials are difficult due to low incidence.

99.7% of CC cases are caused by persistent genital high-risk human papillomavirus (HPV) infection[30]. Current CC cell lines are characterized by different types of HPV. For example, the most famous immortalized cell lines are HeLa – HPV 18, SiHa – HPV 16, CaSki – HPV 16. Also, in C33A and HT-3 cell lines, HPV was not detected. As for primary cultures, the most detected strains are HPV 16 and 18. We showed that in AdMer35 and AdMer43 cells, HPV type 59 is present. Only one cell line, HHUS, described in 2008 by a Japanese group of scientists, was also obtained from epithelial carcinoma of the cervix and had HPV type 59[31]. There are no other registered cell lines with a similar HPV type in the literature.

Due to the fact that the cells were obtained from tumor biopsy material at different stages of the tumor process, they differ in a number of parameters (Table 1).

Immunophenotyping confirmed the epithelial origin of both lines, with AdMer43 showing more pronounced cytokeratin expression. Chromosomal analysis revealed a complex, aneuploid karyotype for both lines, but with distinct ploidy: AdMer35 was predominantly near-tetraploid (modal number 95), while AdMer43 was near-triploid (modal number 77). For comparison, the above-mentioned HHUS cell line (HPV59) was characterized by chromosome number that was distributed the near-diploid pattern, and the modal chromosome number was 48[31]. The same near-triploid set is characteristic of HeLa and SiHa cells[32,33].

Functional characterization revealed pronounced phenotypic differences. AdMer43 exhibited a higher proliferation rate, comparable to HeLa in the initial phase, while AdMer35 proliferated more slowly. Conversely, AdMer35 demonstrated significantly higher migration capacity than AdMer43. Results on Ki67 expression correlate with the proliferation assay, showing very high proliferative potential of AdMer43 cells compared with AdMer35 cells. At the same time, we showed that both cell lines, AdMer35 and AdMer43, are not homogeneous in marker expression.

Different expressions of markers in cells of the same tumor may mirror the heterogeneity of the tumor itself, its clonal evolution, the influence of the tumor microenvironment, and processes of epigenetic variability. Tumors are not homogeneous entities but consist of different cell clones that may have different genetic and epigenetic changes. These changes may lead to different gene expressions and, as a consequence, to different expression of tumor markers[34,35] Both lines formed tumorspheres, indicating the presence of cells with stem-like potential but with distinct morphologies.

Given their origin from the same patient before (AdMer35) and after (AdMer43) radiotherapy, their chemoradiosensitivity was compared. AdMer35 was more sensitive to a single 5 Gy X-ray dose, showing a greater reduction in proliferation, a modest G2/M arrest, and a higher level of late apoptosis compared to AdMer43, while AdMer43 showed minimal apoptosis and no G2/M arrest post-irradiation. Similarly, AdMer43 demonstrated reduced sensitivity to carboplatin and paclitaxel compared to AdMer35, with higher IC_{50} values for both drugs. These phenotypic differences between AdMer35 and AdMer43 likely reflect the treatment-driven selection of more resistant tumor subclones. AdMer43, isolated after two courses of radiotherapy and multiple lines of chemotherapy, showed attenuated G2/M checkpoint response, limited apoptosis after irradiation, and reduced sensitivity to paclitaxel and carboplatin, suggesting a shift in DNA damage response and cell death regulation mechanisms. Such features have been linked to the acquisition of radio- and chemoresistance in cervical cancer, possibly via enhanced DNA repair capacity, epigenetic adaptation, or altered cell cycle checkpoint control[36,37]. This supports the relevance of our paired cell line model for studying resistance mechanisms. Thus, based on the obtained data, we can assume that during the treatment the tumor became less sensitive to the effects of both chemotherapeutic drugs and radiation.

In vivo, both lines were tumorigenic in nude mice. AdMer35 formed larger tumors, consistent with its high migratory activity observed in vitro, suggesting a greater invasive potential. AdMer43 formed smaller tumors but with a higher stromal component and significantly higher Ki-67 positivity, confirming its high proliferative capacity. Thus, the more intensive growth of primary tumor nodes formed by AdMer35 cells is associated with

their high motility and migration activity, causing their ability to invade the surrounding tissues more effectively in vivo. Whereas AdMer43 cells have higher proliferative potential, confirmed by xCELLigence, flow cytometry as well as immunohistochemistry, but a relatively low migrated rate, in vivo, they form smaller, slowly growing tumor nodes compared to AdMer35.

In conclusion, we have successfully established a novel paired cell line model of CC AdMer35 and AdMer43 derived from the same patient before and after chemoradiotherapy. This unique origin is reflected in their divergent phenotypic and genotypic profiles, with AdMer43 displaying features of acquired chemoradioresistance. As one of the very few available CC cell lines bearing HPV type 59, this pair addresses a gap in existing model systems. We propose that the AdMer35/AdMer43 model constitutes a relevant and novel tool for studying the molecular mechanisms underlying therapy resistance and for preclinical evaluation of novel therapeutic strategies aimed at overcoming resistance in cervical cancer.

Materials and methods

Establishment of cervical cancer cell lines

Cervical cancer (CC) samples were obtained from patient biopsy samples. Cervical tissues were aseptically transferred into tubes with Dulbecco's modified Eagle's medium (DMEM) (Servicebio, China) supplemented with 4.5 mg/mL glucose, 3.7 mg/mL sodium pyruvate, antibiotics-antimicotic mix (100 U/mL penicillin, 0.1 mg/mL streptomycin, amphotericin 0.25 µg/mL) (CDH, India) in the absence of fetal bovine serum (FBS) and were kept at 4 °C until processing, which occurred before 4 h. Then the tissues were washed several times under aseptic conditions with pre-cooled Dulbecco's phosphate-buffered saline (D-PBS) (Servicebio, China) containing penicillin 100 U/mL, streptomycin 100 µg/mL and gentamicin 50 µg/mL. Visible vessels and blood clots were removed, and the samples were washed again to remove residual blood.

The samples were fragmented with a scalpel and incubated for 3 h at 37 °C with slow stirring in a 1.5 mL tube containing 1 mL of an enzymatic solution (0.2% collagenase I (Gibco, Thermo Fisher Scientific, USA) and 0.6 U/mL dispase (Gibco, Thermo Fisher Scientific, USA)) in DMEM. After incubation, the samples were centrifuged at 2000 rpm for 7 min, the supernatant was removed, and the pellet was resuspended in 500 µL of keratinocyte medium (Keratinocyte SFM (Gibco, Thermo Fisher Scientific, USA) supplemented with antibiotics (100 U/mL penicillin, 0.1 mg/mL streptomycin and 50 µg/mL gentamicin) and 10% FBS. The cell suspension was transferred to a 12-well plate. After 24 h, the medium was replaced with fresh one, further the medium was changed twice a week. The period from isolation to obtaining a full-fledged primary culture tooks approximately one month. We named these established cell lines as AdMer35 and AdMer43. Once stable growth of the cell culture was achieved, the medium was changed to DMEM containing 10% FBS and antibiotics (100 U/mL penicillin, 0.1 mg/mL streptomycin and 50 µg/mL gentamicin).

Cell cultures and treatments

Human cervical carcinoma cell lines SiHa and HeLa were obtained from the shared research facility "Vertebrate cell culture collection" (Institute of Cytology, RAS, St. Petersburg, Russia). Cells were cultured in DMEM supplemented with 10% (v/v) heat-inactivated FBS and antibiotic-antimycotic mix (100 U/mL penicillin, 100 µg/mL streptomycin and 0.25 µg/mL amphotericin) (hereafter, complete DMEM). Cells were incubated at 37° C in a humidified atmosphere containing 5% CO2 (hereafter, standard conditions).

Before the experiments, cells were detached by 10 min incubation with 300 µL TrypLE Express (Gibco, Thermo Fisher Scientific, USA) and counted with TC20 Automated Cell Counter (Bio-Rad, USA). To maintain cell growth in the exponential phase, cells were passaged twice per week.

Cell irradiation

Cells were seeded on a 6-well plate at a density $2–5 \times 10^5$ cells/well in 2 mL of complete DMEM one day before the experiment. Cells were treated with 5 Gy of X-ray irradiation (225 kV and 30 mA for 1 min with a 0.3 mm Cu filter and 40 × 40 mm collimator) using radiation therapy system SmART+ (Precision X-Ray, USA). After irradiation, the culture medium was changed to a fresh one to avoid contamination. Cells were then detached with 200 µL Cell Dissociation Solution Non-enzymatic 1× (Sigma-Aldrich, USA) and seeded as described below for migration and proliferation assays or incubated for several days for cell cycle analysis and evaluation of apoptosis induction.

Analysis of cell proliferation

Experiments were carried out using the xCELLigence RTCA DP instrument (ACEA Biosciences, USA) in a humidified incubator under standard conditions. Cells were seeded on modified 16-well plates (E-plate 16, ACEA Biosciences, USA) with microelectrodes attached at the bottom of the wells for impedance-based detection of cell attachment, spreading and proliferation of the cells. Initially, 100 µL of cell-free complete DMEM was added to each well. The background was measured after incubation at room temperature for 30 min. Cells in complete DMEM were seeded at a density 5000 cells/well in two replicates; then plates were incubated for additional 30 min before the first point measurement. For the proliferation assay, cells were incubated for 100 h, cell index (CI) was measured every 30 min during the entire period.

Cell migration assay

Cell migration experiments were performed by wound healing assay and using 16-well plates (CIM-16, ACEA, Bioscience, USA), where each well consisted of an upper and lower chamber separated by a microporous membrane. Initially, 160 µL and 30 µL of medium were added to the lower and upper chambers, respectively, and the CIM-16 plate was placed in the RTCA DP device under standard conditions for 30 min for background

measurement. Subsequently, cells were suspended in serum-free DMEM and added to the wells of the upper chamber at a density of 80,000 cells/well. After seeding, the plates were incubated under standard conditions for 30 min and placed in the RTCA DP device. Each sample was seeded in two replicates and measurements were performed every 30 min for 120 h.

For the wound healing assay, SiHa, HeLa, AdMer35, and AdMer43 cells were seeded in triplicate in 6-well plates at a concentration of 500,000 cells per well and allowed to adhere overnight. The cells were then scraped using a 10-µl plastic pipette, washed with PBS, and replaced with complete DMEM medium. Scratches were photographed at 0 and 24 h using an EVOS XL Core microscope. Wound healing was determined by assessing the scratch area at 0 and 24 h point using ImageJ software and normalized to the scratch area at 0 h.

Tumorsphere formation assay

AdMer35 and AdMer43 cells (3×10^5 cells/well) were seeded in ultralow-attachment 6-well plate (Corning, Cambringe, MA, USA) in a tumorsphere medium. The medium consisted of DMEM supplemented with 1% antibiotics/antimycotic, 1% B27 supplement (Gibco, ThermoFisher Scientific, USA), 20 ng/mL epidermal growth factor (SciStore, Moscow, Russia), and 20 ng/mL basic fibroblast growth factor (SciStore, Moscow, Russia). Cells were incubated for 7 days under standard conditions. Every 3 days, 1 mL/well of fresh medium with supplements was added. Imaging of tumorspheres was performed on a Zeiss PrimoVert microscope equipped with AxioCam ERc 5s camera, using Plan-Apochromat 4×/0.10 and 10×/0.30 Ph1 objectives. Image acquisition was performed using ZEN Blue software v. 1.1.1.0 (Zeiss, Germany).

Cytotoxity assays

MTT assay. To determine the cytotoxicity of chemotherapeutic agents the MTT test was used. Cells were seeded in a 96-well plate at a density of 10,000 cells/well for AdMer35 and AdMer43 cells and at a density of 15,000 cells/well for SiHa cells in 100 µL of complete DMEM. Cells were allowed to adhere to the surface for 24 h, then treated with varying doses of paclitaxel (0.01, 0.1, 1, 10 nM) or carboplatin (0.1, 1, 10, 100 nM) and further incubated for 24 h, 48 h, and 72 h. Cells incubated in complete DMEM were used as controls. At the indicated time points 10 µL of MTT solution (5 mg/mL) in DMSO (Sigma-Aldrich, USA) were added to each well and plates were incubated for 2 h under standard conditions. After the incubation medium was removed and 100 µL of DMSO was added to each well to dissolve formazan crystals. Absorbance was measured using a Multiscan RC microplate reader (Thermo Fisher Scientific, USA) at a wavelengths 620 nM for background and 570 nM for formazan. Cells incubated in the absence of compounds were used as control.

LDH assay. The analysis of the toxic effect of radiation on AdMer35 and AdMer43 cells was carried out by quantitative measurement of extracellular lactate dehydrogenase (LDH) using the CyQUAN LDH Cytotoxicity Assay Thermo Fisher kit. At the first step, a calibration curve was obtained. For this purpose, the day before the experiment, cells were seeded at a different density in a 96-well plate: 0; 1×; 3×; 5×; 10×10^3 cells per well in 100 µL of complete DMEM in three replicates and left overnight in an incubator. Then, the conditioned medium from the cells was collected to determine the spontaneous activity and maximum activity (with the addition of lysis buffer) of LDH. The analysis was performed according to the manufacturer's protocol. After that, absorbance at 490 nM and 680 nM was measured and a graph was constructed to determine the linear range of the LDH cytotoxicity assay and the optimal number of cells. In our case, the optimal number of cells was 5×10^3/100 µL of medium. The toxic effect of radiation on cells was evaluated in the second step. Cells were irradiated as described above, seeded at a density 5000 cells/well in a 96-well plate and incubated for 4 or 6 days under standard conditions. Non-irradiated cells were used as a control. Subsequently, analysis was performed as described above. The toxic effect of radiation was calculated as the difference between LDH activity in irradiated cells and spontaneous LDH activity (control) divided by the difference between maximum LDH activity and spontaneous LDH activity. The resulting means are expressed as a percent of cytotoxicity.

Cell cycle analysis

SiHa, HeLa, AdMer35 and AdMer43 cells were seeded in 6-well plates at a density 200,000 cells/well in complete DMEM, irradiated as described above and incubated for 24 h under standard conditions. After incubation both irradiated and control cells were detached as described above, washed with PBS and fixed in cold 75% ethanol. Fixed samples were then stained with 1 µg/mL DAPI (Thermo Fisher Scientific, USA) for 1 h. Fluorescence was captured with NovoCyte 3000 flow cytometer (ACEA Biosciences, USA). The signal was detected in pacific blue channel. Histograms of cell cycle stages distribution were acquired with NovoExpress Software.

Apoptosis detection

SiHa, HeLa, AdMer35 and AdMer43 cells were seeded in 6-well plates at a density 100,000 cells/well in complete DMEM, irradiated as described above and incubated for 5 days under standard conditions. After incubation cells were detached as described above, washed with 1 mL of PBS and stained with Annexin V-FITC/PI cell apoptosis detection kit (Servicebio, China) according to the manufacturer's protocol. Fluorescence was measured with NovoCyte 3000 flow cytometer (ACEA Biosciences, USA). Signals were detected in the FITC and PE-Texas Red channels. Apoptosis graphs were acquired using NovoExpress Software. Cells stained with Annexin V-FITC or PI alone were used for gating the graphs.

Confocal microscopy

Cells were seeded on glass coverslips (Marienfeld, Lauda-Königshofen, Germany) placed in 24-well plates (1.2×10^5 cells/well) in complete DMEM and incubated 24 h under standard conditions for cell adhesion and 80% confluence. Coverslips with cells were washed twice with PBS. Cells were fixed in 4% formaldehyde in PBS for 15 min at 37 °C and then washed twice with PBS. The fixed cells were stained with primary antibodies

(1:100): anti-Cytokeratin (ABclonal, #ARG56129, China), anti-Fibronectin (Abcam, #ab2413, UK) and anti-Ki67 (Abcam, #ab16667, UK) in Stain Buffer for 60 min, followed by staining with secondary antibodies (Goat anti-mouse Alexa Fluor 488, a21121, ThermoFisher, USA or Goat anti-rabbit Alexa Fluor 488, ab 150077, Abcam, UK). After each staining stage, cells were washed twice with PBS and placed on glass slides in DAPI Fluoromount-G mounting media (0100 – 20, SouthernBiotech, Birmingham, AL, USA). Mounted samples were incubated horizontally at room temperature for 18 h in the dark. The morphology of tumor cells was evaluated using a confocal laser scanning microscope LSM710 (Zeiss, Jena, Germany) equipped with a Plan-Apochromat 63×/1.40 Oil DIC M27 objective. Confocal microscopic images were captured using ZEN Black Edition software v. 8.1 (Zeiss, Jena, Germany).

Flow cytometry

The phenotype of CC cells was evaluated by assessing the expression of intracellular markers using flow cytometry. 0.5×10^6 cells were fixed in 2% formaldehyde in PBS for 15 min at room temperature. Cells were then permeabilized with 0.5% BSA, 0.1% Tween-20 in PBS and blocked with 1% BSA and 0.05% Tween- 20 in PBS for 30 min at room temperature. The cells were stained with primary antibodies (1:100) for 30 min at room temperature, followed by staining with secondary polyclonal anti-hIgG- AF488 antibodies (1:1000) for 30 min at room temperature. After each step, the cells were washed twice with FACS buffer, and finally, the cells were resuspended in FACS buffer. Flow cytometry measurements were performed using a NovoCyte 3000 flow cytometer, 10,000 events were acquired for each sample. The data were processed using NovoExpress software v. 1.1.0 (ACEA Biosciences, San Diego, CA, USA). The following anti- human monoclonal antibodies were used: anti-Cytokeratin (ABclonal, #ARG56129, China), anti-Fibronectin (Abcam, #ab2413, UK) and anti-Ki67 (Abcam, #ab16667, UK) .

Assessment of human papilloma virus (HPV)

Cells were seeded in 6-well plates in complete DMEM and incubated under standard conditions until 80% confluence. The cells were then detached and counted. DNA was isolated from 10^6 cells using RealBest DNA Express kits (Vector Best, Russia). Cells were washed with PBS and 400 µL of lysis buffer was added. After the lysis 450 µL of isopropanol containing buffer was added. On the next step 50 µL of magnetic beads suspension was added and the samples were placed on magnetic separator until the beads have pelleted. Supernatant was removed and samples were washed once with 600 µL of washing buffer and twice with 600 µL of ethanol containing buffer. Then the samples were dried at 65 °C for 3 min and DNA was detached from the beads with 100 µL of elution buffer. The resulting eluate was immediately used to evaluate the presence and genotype of HPV in cell cultures. For that purpose, the RealBest DNA HPV PCR kit (Vector Best, Russia) was used to determine the genotypes of HPVs 16, 18, 31, 33, 35, 39, 45, 51, 52, 56, 58 and 59. The principle of analysis is based on recording the amplification process of the selected section of the infectious agent DNA during PCR. For amplification with fluorescent detection in real time, the iQ5 iCycler, CFX96 (Bio-Rad, USA) device was used.

Karyotype analysis

For cytogenetic studies, AdMer35 and AdMer43 cells were incubated in a colchicine solution (1 µg/mL in H2O) under standard conditions for 5 and 10 h. The cells were then separated from the flask surface using a warm EDTA trypsin aqueous solution (0.05%). After this, the cells were hypotonic treated for 20 min (0.56% KCl aqueous solution), then the cells were fixed using a standard fixative (ethanol: acetic acid 3:1). The fixative was changed twice. All centrifugations were performed at 1500 rpm for 8 min. The resulting cell suspension was dropped onto the surface of cold, wet microscope slides and annealed in an alcohol lamp flame. The preparations were then dried and stained with Giemsa dye with preliminary treatment with 0.25% trypsin (GTG staining). Analysis was performed using an OLYMPUS CX41 light microscope (Japan) using 10×, 100× objectives (oil immersion). A video camera and VideoTesT-Kario 3.1 software from Ista-Video Test LLC (Russia, St. Petersburg) were used to record the images. A sufficient number of metaphases were obtained on the preparations, and the chromosome spread in the metaphase plates was good. Metaphase plates with less condensed chromosomes were found on the preparations obtained after colchicine exposure for 5 h. Therefore, analysis was performed on these preparations. Fifty metaphase plates were analyzed. Round, separately lying plates were selected for the analysis. The number of chromosomes in each plate was counted.

Mice

Four-to-six-week-old female athymic Nude mice with average weight of 20–22 g were obtained from the Center for Genetic Resources of Laboratory Animals at the Institute of Cytology and Genetics of the Siberian Branch of the Russian Academy of Sciences (SB RAS) (Novosibirsk, Russia). Mice were kept in plastic cages (3 animals per cage) under a normal daylight schedule in temperature-controlled, specific pathogen-free conditions. Water and food were provided *ad libitum*. Mice were euthanized at the end of experiment under isoflurane anesthesia using a gas mixture containing 3% isoflurane and 97% air at a flow rate of 2 L/min.

Tumor transplantation and animal experiment design

AdMer35 and AdMer43 cells were cultured under standard conditions. Before detachment, the cells were washed twice with PBS, detached using TripLE (Gibco, Thermo Fisher Scientific, USA) then pelleted by centrifugation at 2000 rpm and resuspended in saline buffer. AdMer35 and AdMer43 cells at dose of 2 or 3×10^6 cells per mouse in 150 µL of saline buffer were subcutaneously (s.c.) implanted into the left flank of athymic Nude mice ($n = 3$ for AdMer 35 at both doses and for AdMer43 at a dose of 2×106 cells per mouse; $n = 4$ for AdMer43 at a dose of 3×10^6 cells per mouse). During the experiment, the tumor volumes were determined twice a week using caliper measurements and were calculated as $V = (D \times d^2)/2$, where D is the longest diameter of the tumor node and d

is the shortest diameter of the tumor node perpendicular to D. Mice were sacrificed on day 21 after tumor cell implantation and tumor nodes were collected for subsequent histological analysis.

Histology and immunohistochemistry analysis

For the histological study, the tumor specimens were fixed in 10% neutral-buffered formalin (BioVitrum, Moscow, Russia), dehydrated in ascending ethanols and xylols, and embedded in HISTOMIX paraffin (BioVitrum, Russia). Paraffin sections (up to 5 µm) were sliced on a Microm HM 355 S microtome (Thermo Fisher Scientific, USA) and stained with hematoxylin and eosin. Connective tissue fibers were stained with van Gieson staining.

For the immunohistochemical study, the tumor sections ($n = 3$ for both groups at dose of 2 and 3×10^6 cells per mouse) were deparaffinized and rehydrated. Antigen retrieval was performed after exposure in a microwave oven at 700 W. The samples were incubated with anti-Ki-67 (#ab16667, Abcam, Boston, MA, USA) and anti-Cytokeratin (ABclonal, #ARG56129, China) primary antibodies according to the manufacturer's protocol. Then, the sections were incubated with secondary horseradish peroxidase (HPR)-conjugated antibodies, exposed to the 3,30-diaminobenzidine (DAB) substrate (Rabbit Specific HRP/DAB (ABC) Detection IHC Kit, ab64261, Abcam, USA), and stained with Mayer's hematoxylin.

Morphometric analysis of tumor sections included evaluation of the numerical density (Nv) of mitoses and Ki-67-positive cells indicating the number of particles studied in the square unit, 3.2×10^6 µm^2 in this case. Ten to fifteen random fields were examined from the tumor specimens of three mice in each group, forming 30–45 test fields for a total. Mitotic and Ki-67-positive cells counting was performed at magnification ×400.

All images were examined and scanned using an Axiostar Plus microscope equipped with an Axiocam MRc5 digital camera (Zeiss, Oberkochen, Germany) at magnification of ×200 and ×400.

Statistical analysis

Each experiment was performed in triplicate under identical conditions. Data are shown as mean ± standard deviation. Differences between test and control samples were analyzed using the Student's t-test, and in vivo data were analyzed using the Mann-Whitney U test, with a p-value of less than 0.05 considered statistically significant.

Data availability

The data used and analyzed in the present study are available from the corresponding author on reasonable request.

Received: 2 July 2025; Accepted: 12 January 2026
Published online: 04 February 2026

References

1. Bray, F. et al. Global cancer statistics 2022: GLOBOCAN estimates of incidence and mortality worldwide for 36 cancers in 185 countries. *CA Cancer J. Clin.* **74**, 229–263 (2024).
2. Yang, M. et al. Global trends and age-specific incidence and mortality of cervical cancer from 1990 to 2019: an international comparative study based on the global burden of disease. *BMJ Open* **12**, (2022).
3. He, W. Q. & Li, C. Recent global burden of cervical cancer incidence and mortality, predictors, and Temporal trends. *Gynecol. Oncol.* **163**, 583–592 (2021).
4. Liu, Y. & Zheng, W. Cervical cancer Development, Screening, and prevention. *Gynecol. Obstet. Pathol.* **1–16** https://doi.org/10.1007/978-981-19-7696-4_52-1 (2024).
5. Petrelli, F. et al. Human papillomavirus (HPV) types 16 and 18 infection and esophageal squamous cell carcinoma: a systematic review and meta-analysis. *J. Cancer Res. Clin. Oncol.* **147**, 3011–3023 (2021).
6. Malagón, T., Franco, E. L., Tejada, R. & Vaccarella, S. Epidemiology of HPV-associated cancers past, present and future: towards prevention and elimination. *Nat. Rev. Clin. Oncol.* **21**, 522–538 (2024).
7. Zhang, S., Xu, H., Zhang, L. & Qiao, Y. Cervical cancer: Epidemiology, risk factors and screening. *Chin. J. Cancer Res.* **32**, 720–728 (2020).
8. Pujade-Lauraine, E. et al. Comparison of global treatment guidelines for locally advanced cervical cancer to optimize best care practices: A systematic and scoping review. *Gynecol. Oncol.* **167**, 360–372 (2022).
9. Massobrio, R. et al. New frontiers in locally advanced cervical cancer treatment. *J. Clin. Med.* **13**, 4458 (2024).
10. Noy, M. A. et al. Levels of evidence for radiation therapy recommendations in the National comprehensive cancer network (NCCN) clinical guidelines. *Adv. Radiat. Oncol.* **7**, 100832 (2021).
11. Siegel, R. L., Miller, K. D., Wagle, N. S. & Jemal, A. Cancer statistics, 2023. *CA Cancer J. Clin.* **73**, 17–48 (2023).
12. Capes-Davis, A. Database of Cross-Contaminated or misidentified cell lines international cell line authentication committee (ICLAC). (2013).
13. Makowska, A., Kontny, U. & Weiskirchen, R. HeLa cells cross-contaminated nasopharyngeal carcinoma cell lines: still a common problem. *Br. J. Cancer*. **130**, 1885–1886 (2024).
14. Jäger, W. et al. Hiding in plain view: genetic profiling reveals decades old cross contamination of bladder cancer cell line KU7 with HeLa. *J. Urol.* **190**, 1404–1409 (2013).
15. Di Fiore, R. et al. Cancer stem cells and their possible implications in cervical cancer: A short review. *Int. J. Mol. Sci.* **23**, 5167 (2022).
16. Wen, G. M., Xu, X. Y. & Xia, P. Metabolism in Cancer Stem Cells: Targets for Clinical Treatment. *Cells* **11**, 3790 (2022).
17. Ishikawa, M. et al. Simultaneous expression of cancer stem cell-like properties and cancer-associated fibroblast-like properties in a primary culture of breast cancer cells. *Cancers (Basel)*. **6**, 1570–1578 (2014).
18. Tucker, K. et al. Defining the learning curve for successful staging with Sentinel lymph node biopsy for endometrial cancer among surgeons at an academic institution. *Int. J. Gynecol. Cancer*. **30**, 346–351 (2020).
19. Liu, Y., Cao, C., Zhai, P. & Zhang, Y. Biological characteristics of cervical precancerous cell proliferation. *Open. Med. (Warsaw Poland)*. **14**, 362–368 (2019).
20. Darroudi, F. et al. PCC and COBRA-FISH a new tool to characterize primary cervical carcinomas: to assess hall-marks and stage specificity. *Cancer Lett.* **287**, 67–74 (2010).

21. Deng, H., Mondal, S., Sur, S. & Woodworth, C. D. Establishment and optimization of epithelial cell cultures from human ectocervix, transformation zone, and endocervix optimization of epithelial cell cultures. *J. Cell. Physiol.* **234**, 7683–7694 (2019).
22. Scholzen, T. & Gerdes, J. The Ki-67 protein: from the known and the unknown. *J. Cell. Physiol.* **182**, 311–322 (2000).
23. Kumar, P., Nagarajan, A. & Uchil, P. D Analysis of cell viability by the lactate dehydrogenase assay. *Cold Spring Harb Protoc.* **2018**, 465–468 (2018).
24. Koukourakis, M. I. & Giatromanolaki, A. Warburg effect, lactate dehydrogenase, and radio/chemo-therapy efficacy. *Int. J. Radiat. Biol.* **95**, 408–426 (2019).
25. Stark, G. R. & Taylor, W. R. Control of the G2/M transition. *Mol. Biotechnol.* **32**, 227–248 (2006).
26. Yan, Y., Black, C. P. & Cowan, K. H. Irradiation-induced G2/M checkpoint response requires ERK1/2 activation. *Oncogene* **26**, 4689–4698 (2007).
27. Kim, B. M. et al. Therapeutic implications for overcoming radiation resistance in cancer therapy. *Int. J. Mol. Sci.* **16**, 26880–26913 (2015).
28. Tanaka, T. et al. Patient-Derived xenograft models in cervical cancer: A systematic review. *Int. J. Mol. Sci.* **22**, 9369 (2021).
29. Lõhmussaar, K. et al. Patient-derived organoids model cervical tissue dynamics and viral oncogenesis in cervical cancer. *Cell. Stem Cell.* **28**, 1380–1396e6 (2021).
30. Okunade, K. S. Human papillomavirus and cervical cancer. J. Obstet. Gynaecol. 40 602–608 at (2020). https://doi.org/10.1080/01443615.2019.1634030
31. Ishiwata, I. et al. Establishment and characterization of human uterine cervical epidermoid carcinoma cell line HHUS containing HPV 59 DNA. *Hum. cell. Off J. Hum. Cell. Res. Soc.* **17**, 151–156 (2004).
32. Frattini, A. et al. High variability of genomic instability and gene expression profiling in different HeLa clones. *Sci. Rep. 2015*. **51** (5), 1–9 (2015).
33. Ng, G., Huang, J., Roberts, I. & Coleman, N. Defining Ploidy-Specific thresholds in array comparative genomic hybridization to improve the sensitivity of detection of single copy alterations in cell lines. *J. Mol. Diagn.* **8**, 449 (2006).
34. Meacham, C. E. & Morrison, S. J. Tumor heterogeneity and cancer cell plasticity. *Nature* **501**, 328 (2013).
35. The Genetics of Cancer - NCI. https://www.cancer.gov/about-cancer/causes-prevention/genetics
36. Xing, J. L. & Stea, B. Molecular mechanisms of sensitivity and resistance to radiotherapy. *Clin. Exp. Metastasis*. **41**, 517–524 (2024).
37. Alamilla-Presuel, J. C., Burgos-Molina, A. M., González-Vidal, A., Sendra-Portero, F. & Ruiz-Gómez, M. J. Factors and molecular mechanisms of radiation resistance in cancer cells. *Int. J. Radiat. Biol.* **98**, 1301–1315 (2022).

Acknowledgements

The authors thank Albina V. Vladimirova (Institute of Chemical Biology and Fundamental Medicine SB RAS, Novosibirsk, Russia) for cell maintenance.

Author contributions

EL, IT: designing of the study; SK, ES: obtaining of biopsy samples from patients; IT EL: processing of biopsy samples; VT, DM, IT, EL: performing the experiments and analyzed the results in cell culture; AS: performing and analyzing the results of in vivo experiments; OP : cells irradiation; OM: performing confocal microscopy; TG: performing chromosome analysis; EB: performing of assessment of HPV; EL, IT, VT, MZ: writing—review and editing; MZ: funding acquisition, resources, supervision. All authors revised the final version of the manuscript and agreed to this submission.

Funding

This work was supported by the Russian Science Foundation (grant number 19-74-30011) and by the Russian state-funded project for ICBFM SB RAS (grant number 125012300659-6).

Declarations

Competing interests

The authors declare no competing interests.

Ethical approval

The study was approved by the Ethics Committee of the Institute of Chemical Biology and Fundamental Medicine (No 1 from January 11 2022), with the patient's informed consent, and conducted according to the Declaration of Helsinki. All animal procedures were carried out in strict accordance with the European Communities Council Directive 86/609/CEE. The experimental protocol was approved by the Committee on the Ethics of Animal Experiments at the Institute of Cytology and Genetics SB RAS (protocol no. 111 of 7 December 2021). This study was also conducted in accordance with the guidelines of the Animal Research: Reporting of In Vivo Experiments (ARRIVE).

Additional information

Supplementary Information The online version contains supplementary material available at https://doi.org/10.1038/s41598-026-36260-4.

Correspondence and requests for materials should be addressed to E.L.

Reprints and permissions information is available at www.nature.com/reprints.

Publisher's note Springer Nature remains neutral with regard to jurisdictional claims in published maps and institutional affiliations.